URTeC: 208

Frac Hit Prevention and Engineered Treatment Design in the Permian Basin Using In-Situ Stress from 3D Seismic

Michael Shoemaker*[1], James Hawkins[1], John Becher[1], Veronica Gonzales[1], Sandeep Mukherjee[1], Reza Garmeh[1], David Kuntz[1]; 1. Callon Petroleum Company

Abstract

E&P companies in the Permian Basin typically implement basin-wide development strategies that involve cookie-cutter type methods that use multi-well pads with identical geometric stage and cluster spacing. Such development strategies however fail to recognize and account for subsurface stress heterogeneity, and thus assume similar geomechanical properties that are homogeneous and isotropic which may cause well-to-well interference or “frac hits”, particularly near “parent” wells as fields continue to mature.

Minimum horizontal stress (S_h) is the leading parameter that controls hydraulic fracture stimulation, but is next to impossible to measure quantitatively, especially far field and in 3D space. In-situ stress differences from fluid depletion, combined with stratigraphy and subsequent mineralogy contrasts, control fracture containment vertically and laterally which define fracture propagation and complexity. Far field preference of virgin rock towards brittle vs ductile deformation is governed by mineralogy which defines the elastic moduli or geomechanical behavior of the rock. When integrated with pore pressure and overburden stress, the elastic rock properties are characterized by the Mechanical Earth Model (or MEM) which defines key inputs for calculating S_h using the uniaxial Ben Eaton stress equation. However, implementing this model historically produces incorrect calculated stress, when compared to field measured stress, due to an assumed homogeneous and isotropic subsurface.

Parameterization of fracture geometry models for well spacing, frac hit mitigation, and engineered treatment design in shale (or mudrock) requires an anisotropic in-situ stress measurement that accurately captures subsurface stress states. A method herein is proposed that achieves this using a modified version of the anisotropic Ben Eaton stress equation. The method calculates minimum horizontal stress by substitution of AVO seismic inversion volumes directly into the stress equation, replacing the bound Poisson’s ratio term with an equivalent anisotropic corrected Closure Stress Scalar (CSS) defined in terms Lamé elastic parameters, specifically lambda (λ) or incompressibility and mu (μ) for shear rigidity. The CSS volume is corrected for anisotropy using static triaxial core, and is calibrated to multi domain data types including petrophysics, rock physics, completion engineering, and reservoir engineering (DFIT) measurements.

Successful application of said method in the Delaware and Midland sub-basins (of the greater Permian Basin) is shown. Anisotropic minimum horizontal stress (S_h) volumes from 3D seismic defined at 1 ft. vertical log resolution were interpreted quantitatively regionally, particularly as a prevention tool near parent wells prone to frac-hits. Moreover, the method provides an anisotropic measurement of in-situ stress variability (or stress differential) to qualitatively model 3D fracture geometries for engineered treatment optimization. Current stress modeling methods rely on the propagation of geomechanical properties from well control, which do not necessarily represent rock properties and stress states at the area of interest.

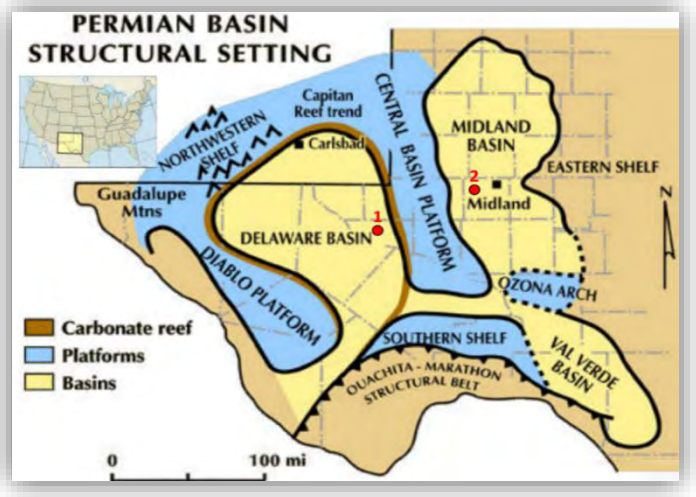

Figure 1. Permian Basin locator with structural features and study areas (modified form Bureau of Economic Geology).

Permian Basin field Development

Technological advancements in horizontal drilling and hydraulic fracture stimulation of tight oil formations have resulted in the resurgence of the century-old Permian Basin (Figure 1). Published data from the Energy Information Administration (EIA) show that the U.S. Permian recently produced 4.1 million barrels / day (EIA, 2019), which surpasses any basin in the world. In fact, the EIA predicts total U.S. crude oil production will average 11.7 million b/d in 2019 which would surpass the previous production record of 9.6 million b/d set in 1970 (EIA, 2018). More than half of this production growth is projected to come from tight oil produced from the Permian Basin. That said, longer term production growth however, may be hindered by "parent-child" or well-to-well interference (Jacobs, 2019), resulting in less production and steeper decline curves from suboptimal frac jobs. Data suggests the problem may worsen for operators in the Permian as the number of child wells has now reached 50% (Cunningham, 2018) as operators continue to practice more simplified cookie-cutter type development methods.

E&P companies in the Permian Basin currently implement basin-wide development strategies that involve "harvesting" or cookie-cutter type methods that use multi-well pads to drill stacked horizontal layers. This simple approach uses a repeated sequence implementing identical geometric stage placement and pumping schedules (Shoemaker, et al., 2015). Such development strategies however fail to recognize subsurface rock properties and subsequent stress heterogeneity, which assume similar geomechanical properties that are homogeneous and isotropic. Hydraulic fracture initiation and fracture geometry however are defined by in-situ stress variability, the extent of which defines well economic performance. Assumed isotropic stress states can result in suboptimal hydraulic fracture geometry modeling and treatment design, in addition to near well frac hits. This can result in well underperformance, particularly as operators continue to develop pads near older (parent) laterals as fields mature. Resultant stress variability from produced fluid depletion or from lithology changes can cause asymmetric fracture geometries (Meta and Gonzales, 2014) which can alter (child) well performance and ultimate recovery by as much as 25% (Cherian, et al., 2018). In addition to parent-child issues, some workers have even reported that on average 30% of the perforation clusters in shale rocks are unproductive (Miller, et al., 2011), further demonstrating the need for improved development strategies that account for subsurface variability (Warpinski, et al., 1987).

Other than diagnostic methods, current attempts to mitigate production quandaries in the Permian involve subsurface technology focused with well spacing and engineered fracture treatment design. This requires

hydraulic fracture geometry modeling with field measured subsurface stress inputs. Current methods use an integrated multi-domain modeling workflow approach referred to as "seismic-to-simulation" as presented by (Cippola, et al., 2011) and (Cherian, et al., 2015, 2018) which is an iterative process centered about fracture geometry modeling. Although marginally successful, these methods still rely on the propagation of geomechanical properties away from vertical well control, which do not necessarily represent local rock properties at the area of interest. An amended seismic-to-simulation workflow was adopted for this study that includes the seismic method presented herein (specifically, steps 2 through 6), and follows in ascending order of input:

1. **Petrophysical Modeling-** Calculate mineralogy compositions, porosity, and saturation models in defining mechanical lithofacies for reservoir and completion quality classification (Cherian et al., 2015).
2. **Seismic Interpretation**- Integrate and tie 3D seismic data to formation tops in time, and convert the seismic horizons / framework to depth for structural and thickness preservation at well control (Shoemaker, et al., 2006).
3. **Rock Physics Modeling**- Define quantitative elastic seismic response to petrophysics and subsequent mineralogy compositions for reservoir and completion quality, integrating lithofacies classification (Dvorkin and Nur, 1996, Vernik and Milovac, 2011).
4. **Geologic Modeling**- Construct 3D geo-model to propagate lithofacies via seismic framework in depth using well control and stochastic algorithms (Cherian, et al., 2018).
5. **Geomechanics-** Calibrate geomechanical properties from 3D seismic to logs and core (Shoemaker, et. al, 2018, 2019), and to Diagnostic Fracture Injection Test (DFIT) data using the modified Ben Eaton anisotropic model to estimate near wellbore and far field minimum horizontal in-situ stress (Ganpule, et al., 2015).
6. **Fracture Modeling**- Estimate fracture geometry using calculated stress as input to numerical planar fracture simulators, which integrate petrophysics with geomechanics, to history match field measured fracture treatment pressures (Azad, et al., 2017), and calibrate to microseismic if available.
7. **Completion Modeling-** Run sensitivities for optimal well spacing and fracture stimulation parameterization which includes proppant and fluid type, horizontal cluster spacing, diverters, and stage length (Meta and Gonzales, 2014).
8. **Reservoir Modeling-** Reservoir simulation and forecasting via iterative history matching of fluid production calibrated to the completion modeling (Cherian, et al., 2018).

Permian Basin Geology

The Midland and Delaware sub-basins (Frenzel, et al., 1988) of the greater Permian Basin (Figure 1) share mutual characteristics such as age and lithology, but depths, stratigraphy, and nomenclature vary significantly (Galloway, et al., 1983). The focus of this study includes both sub-basins which demonstrate a high degree of vertical and lateral heterogeneity within the Spraberry, Bone Spring, and Wolfcamp formations where horizontal wells are landed and fraced within just a few hundred vertical feet of each other, and typically developed implementing the aforementioned harvesting or cookie-cutter type approach. Heterogeneity of rock properties results from the irregular stacking of discrete depositional carbonate units resulting in varying mineralogy compositions (Hobson, et al., 1985) which influence elastic geomechanical properties that ultimately define in-situ stress states and fracture complexity.

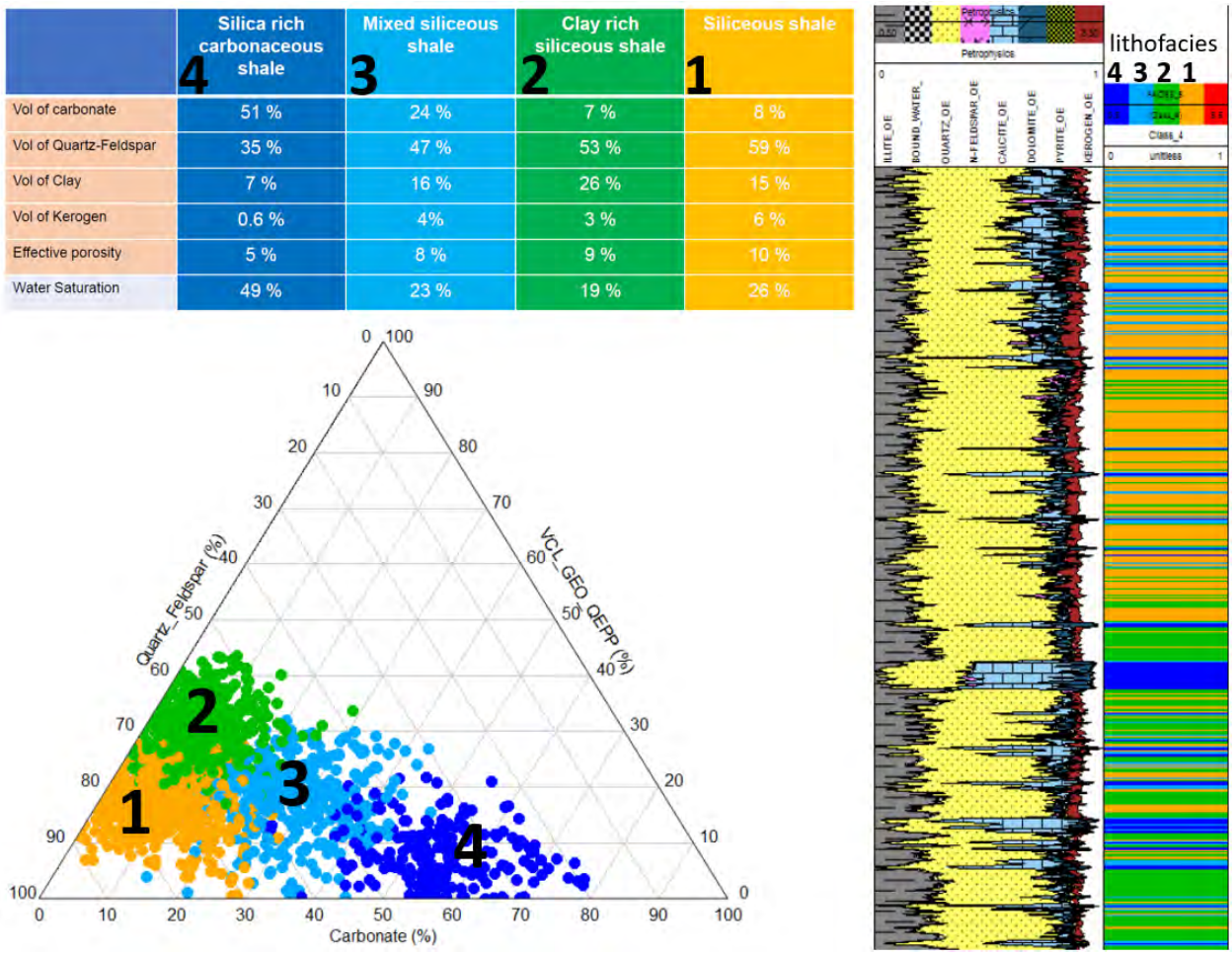

Figure 2. Ternary diagram showing lithofacies classification from petrophysics modeling representing the Delaware Basin study area (Figure 1). The Wolfcamp section is shown. Lithofacies (1 to 4) ascend in increasing order of brittleness (less clay and organics), and are integrated with the rock physics templates shown in Figure 3.

The Spraberry, Bone Spring, and Wolfcamp formations are highly anisotropic kerogen-rich dark shales and interbedded detrital carbonates, muds, and sands that were deposited predominately by debris / gravity flows and turbidity currents down slope from the Central Basin Platform or CBP (Figure 1), and likely were deposited in a proximal basin plain environment (Wilson, 1975). Shelf-ward toward the CBP, carbonate deposition increases with decreasing anisotropy to a point where large detached blocks of dolostone are common proximal to the platform margin (Mazzullo and Reid, 1987). Conceptually, the detrital flows define fairways that have increased carbonate mineralogy compositions with proportionally less organics and clay, and therefore are mechanically less ductile and represent locations that are potentially less anisotropic and more conducive to hydraulic fracture stimulation. These mineralogical changes in lithofacies drive fracture geometry and completion optimization, and represent areas of in-situ stress variability that the seismic method, presented herein, attempts to measure away from vertical well control.

For both sub-basins, the elastic seismic response to lithofacies was characterized using petrophysics models integrated with rock physics templates shown in Figures 2 and 3, respectively for the Delaware Basin and combined in Figure 10 for the Midland Basin. Petrophysics models and subsequent lithofacies, defined by a ternary mineralogical distribution plots, were generated using static core and dynamic quad combo data. For the Midland study area, the Spraberry and Wolfcamp formations were commingled and

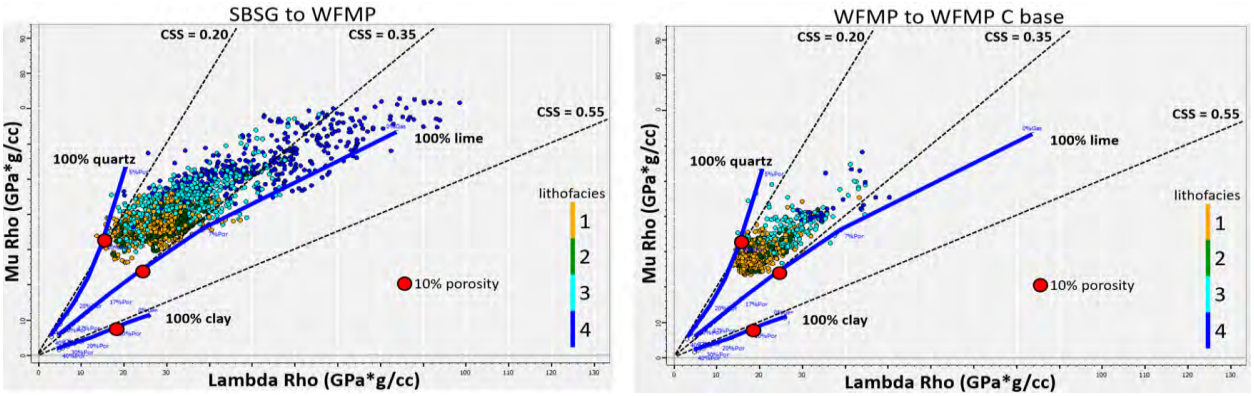

Figure 3. Rock physics templates, calibrated to the Delaware Basin stud area, representing the Bone Spring formation (left) and Wolfcamp formation (right) that show multi-domain relationships between geomechanical properties Lambda-Mu-Rho (LMR) with respect to changes in CSS, lithofacies (Figure 2), and porosity (Figure 4). Lower CSS typically results in optimal landing zones. Notice the significant addition of lime in the Bone Spring that can also act as stress barriers to propagating fractures (higher magnitude of CSS).

grouped into five separate geomechanical lithofacies based on clustering of stratigraphic and mineralogical changes, and listed in ascending order of increasing "brittleness".

The Delaware Basin is characterized by four lithotypes, also in ascending order of brittleness but based on the commingling of the Bone Spring and Wolfcamp formations (Figure 2). However, due to increased formation thickness and contrasting rock properties, individual rock physics templates, representing each formation (Figure 3) were used. For both basins, quantified elastic seismic response to geomechanical properties, and thus in-situ stress states, were analyzed combining said lithofacies with rock physics templates (Vernik, 2016). A lambda-rho versus mu-rho RPT (Figures 3 and 10) was created using Hashin-Shtrikman based bounds (Dvorkin and Nur, 1996) with identical mineralogical elastic constants defined by Sayers et al. (2015).

In Situ Stress and Geomechanics

In-situ stress state is the most important factor that controls hydraulic fracture stimulation and complexity (Iverson, 1995; Warpinski, et al., 1987), but is next to impossible to measure quantitatively, especially far

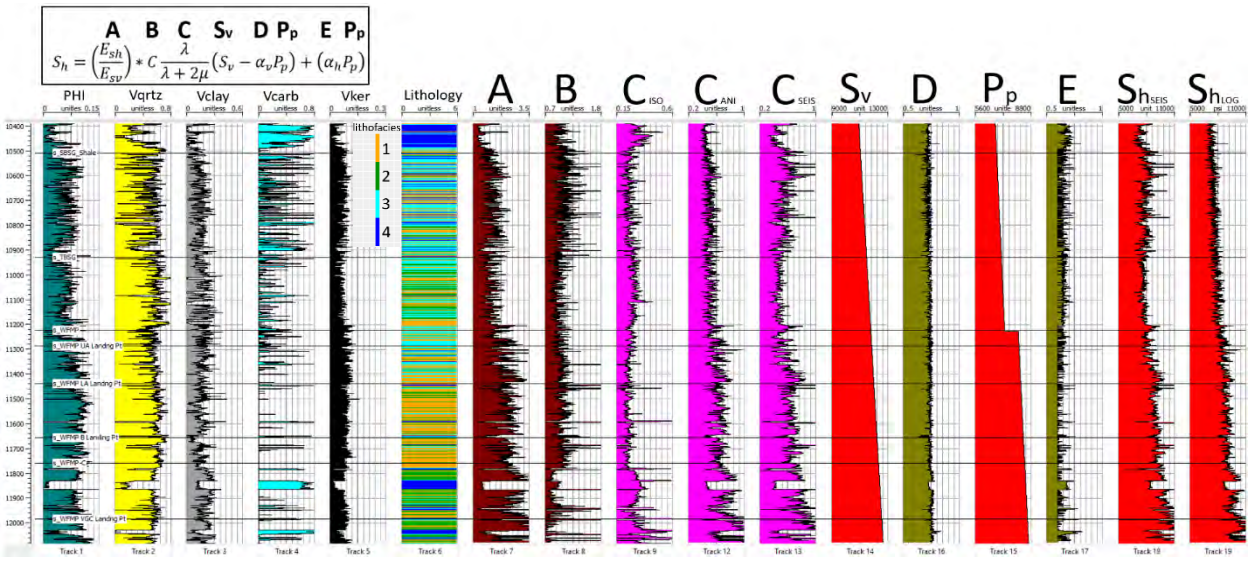

Figure 4. 1D Mechanical Earth Model (or MEM) representing the Delaware Basin example with the uniaxial strain equation for minimum horizontal stress. Equation terms are labeled and defined by the curves used to interpolate the cubes shown in Figure 5. Lithology based on mineralogy and facies classification is defined in Figure 2. A full suite of logs, including sonic scanner and over 1,500 ft. of core were acquired in the vertical pilot hole representing the lateral wellbore shown in Figure 8.

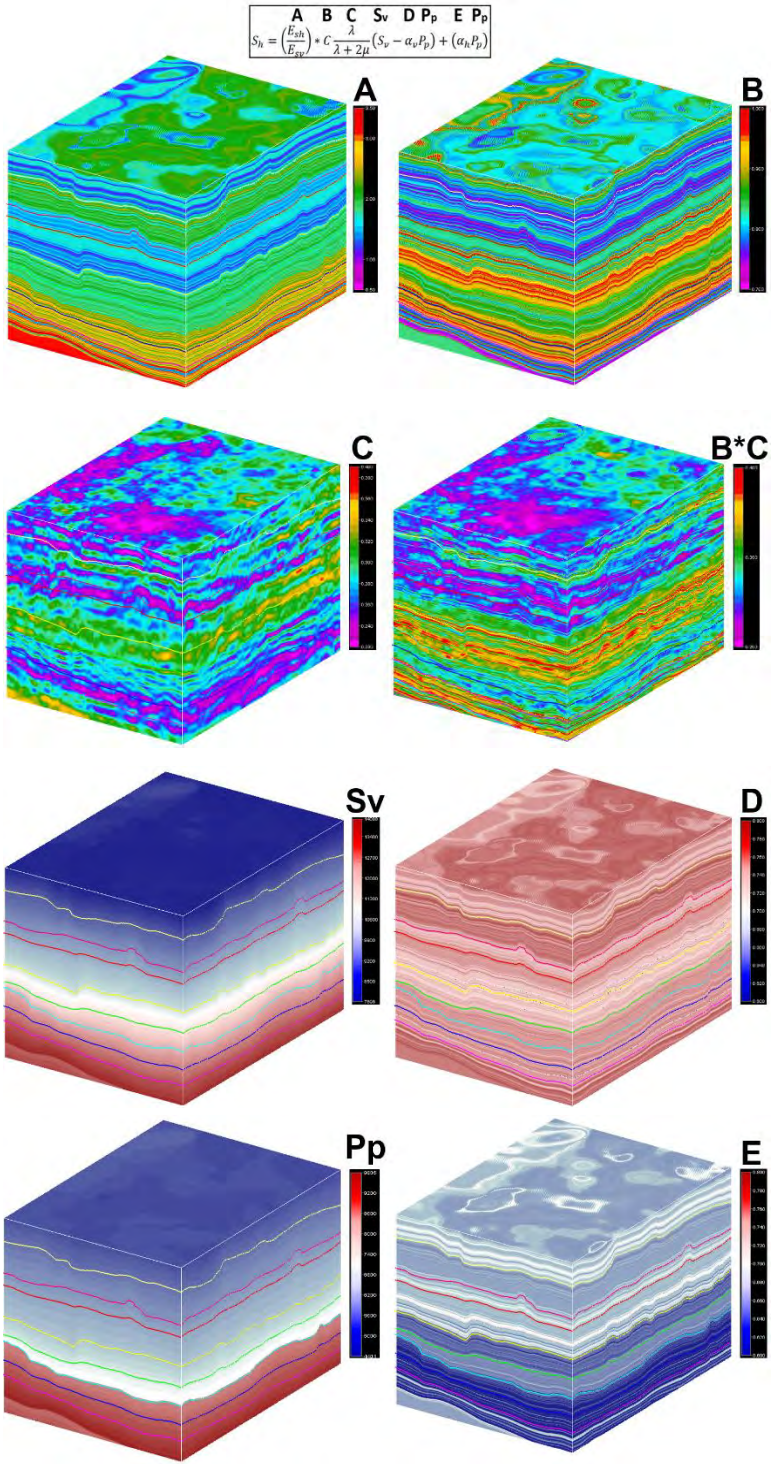

Figure 5. 3D cubes from the Delaware Basin study area representing each of the seven uniaxial stress equation terms defined by the MEM in Figure 4. The calculated minimum horizontal stress cube, using the associated cubes above, is shown in Figure 6. Notice the additional anisotropic variability after the term B cube is integrated with the seismic cube (terms B*C). Each cube is approximately 30 miles square.

field and away from the wellbore in 3D space. Minimum horizontal stress (S_h) is one of three principle stresses that describe the subsurface stress state, and its magnitude controls the propagation of hydraulic fracture stimulation (Ma and Holditch, 2016) which ultimately determines the success of a well and its economic performance. When induced injection pressures exceed S_h, fractures generally occur, and will propagate orthogonally toward the direction of S_h within a path of least resistance determined by stratigraphic (or geomechanical) contrasts. In-situ stress differences between bedding planes control fracture containment vertically and laterally, which defines the complexity of fracture propagation and fracture geometry characteristics such as height growth, length, and width which ultimately control proppant placement, drainage, and well spacing (Ganpule, et al., 2015). Geomechanical rock properties from mineralogical compositions define elastic behavior and tensile strength influencing how the subsurface will deform under induced stress and strain which are governed by elastic rock properties such as Young's Modulus, Poisson's ratio and Biot's coefficient.

The Mechanical Earth Model

When combined with pore pressure and overburden stress, the elastic properties describe the Mechanical Earth Model (or MEM) which characterizes the geomechanical behavior of the subsurface. The MEM (Figure 4) acts as both a diagnostic and predictive tool defining key inputs for calculating minimum horizontal stress using an isotropic uniaxial strain based model defined in terms of the Ben Eaton stress equation which has been commonly used by geoscientists for decades to calculate subsurface

stress. However, calculated S_h from this simple model historically produces uncertain results (Barree, et al., 2009), when compared to field measured stress (Iverson, 1995), due to an assumed homogeneous and isotropic subsurface. This is particularly contrary to tight oil formations which represent shale (or mudrock) reservoirs that are highly variable and laminated, and are anisotropic representing Vertical Transverse Isotropic media (VTI) (Sayers, 2010). Likewise, more complex models require rock parameterization based on laboratory (static core) measurements (Thierceline, 1992 et al.; Singleton, 2018a), but quantitative geomechanical measurements are rare to obtain. This reflects a current inability to accurately predict far field in-situ stress (Iverson, 1995) for fracture geometry estimation and effective hydraulic fracture treatment design that accounts for far field virgin subsurface variability.

Closure Stress Scalar (CSS)

The CSS represents a unique elastic rock property also characterized by the MEM (Figure 4), but defined as a function of Lamé elastic constants (Goodway, et al., 2010; Close, et al., 2012, Perez, et al., 2012), where lambda (λ) is incompressibility and mu (μ), shear modulus. The calculated CSS results in improved vertical and lateral geomechanical variability (Goodway, et al., 1997, 2014) along horizontal wellbores and far field, and is ultimately corrected for anisotropy using static triaxial core (Higgins, et al., 2008). The CSS is equivalent to the bound Poisson's ratio term ($\frac{\upsilon}{(1-\upsilon)}$), also referred to as the stress coupling factor (Vernik and Milovac, 2011), that is embedded in the *isotropic* Ben Eaton model (or uniaxial stress equation) historically used to calculate minimum horizontal stress:

$$S_h = \frac{\upsilon}{(1-\upsilon)}\left(S_v - \alpha P_p\right) + \alpha P_p, \quad (1)$$

where S_h equals the induced stress required to fracture the rock given υ or Poisson's ratio, the overburden stress (Sv), Biot's coefficient (α), and pore pressure of the formation (Pp). For CSS, Lambda (λ) and mu (μ) define Hooke's law relating stress to strain (Sayers, 2010) which intrinsically defines the fracability of "brittle" (low stress) rocks and ductile (higher stress) rocks. Likewise, Goodway et al. (2010) and Close et al. (2012) define the closure stress scalar in terms of λ and μ, which is equivalent to the bound Poisson's ratio term defined in Equation 1 or:

$$CSS_{ISO} = \frac{\lambda}{\lambda+2\mu} = \frac{\upsilon}{(1-\upsilon)}, \quad (2)$$

where CSS represents an isotropic rock quality term calculated quantitatively from the AVO seismic inversion, discussed below.

Method

A process herein is proposed that has successfully measured far field in-situ stress states using a modified version of the anisotropic Ben Eaton stress model presented by Narasimhan et al. (2016) and amended to the "seismic-to-simulation" workflow defined by Cippola et al. (2011) and Cherian et al. (2018). The new model calculates minimum horizontal stress (S_h) by substitution of prestack simultaneous inverted 3D seismic (Gray et al., 2000; Singleton, 2018b) volumes or cubes (Figure 5) directly into the uniaxial stress equation by replacing the bound Poisson's ratio term with an equivalent Closure Stress Scalar (CSS) term extracted from surface seismic data.

A model based simulated annealing numerical method was implemented for the elastic (AVO) seismic inversion which was ultimately used to calculate the CSS. An Aki and Richards (1980) linearized approach to approximate Zoeppritz (1919) equations was used to generate elastic geomechanical properties including broadband compressional wave velocity (Vp) and shear wave velocity (Vs) which were used to calculate Poisson's ratio from the seismic. Prestack common midpoint gathers were conditioned to enhance signal-to-noise. For added sensitivity to vertical and horizontal in-situ stress variability, inverted elastic parameters were recast into equivalent terms of Lamé elastic constants (Goodway, et al., 1997, 2010, 2014; Close, et al., 2012; Sayers et al., 2015, Perez, et al., 2012) defined by lambda (λ) or incompressibility and mu (μ) for shear rigidity, and were used to calculate the closure stress scalar.

CSS volumes derived from the AVO seismic inversion were calibrated and quantitatively interpreted using the rock physics templates, defined in Figures 3 and 10 for the Delaware and Midland Basins, respectively. Constant lines of CSS, calculated from dynamic log data, were used to characterize the geomechanical seismic response to mineralogy compositions.

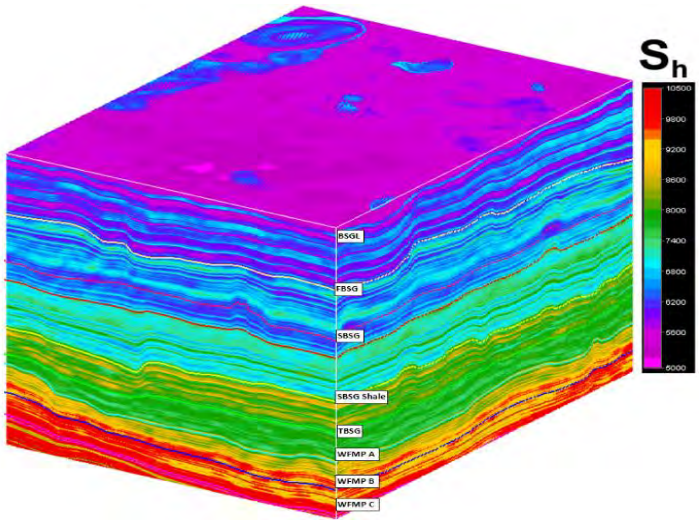

Figure 6. Minimum horizontal stress cube (S_h), approximately 30 miles square.

Anisotropic Correction Scalar

For Vertical Transverse Isotropic (VTI) media representing anisotropic shale, Thomsen et al. (2013) and Sayers et al. (2015) both argue that the industry needs to integrate anisotropy effects into seismic methods that are currently being implemented to extract geomechanical and stress properties from shale. Local anisotropy effects used herein were investigated and measured using dynamic compressional sonic and shear logs calibrated to static triaxial core data (Barree, et al., 2009) from the area. Narasimhan et al. (2016) provides a valid workflow, implementing a Ben Eaton anisotropic stress model for converting static mechanical measurements from core to dynamic velocity measurements using empirical models calibrated to the area. Resulting anisotropic scalars, representing correction factors to isotropic terms defined in Equation 2, are defined in Equation 3:

$$S_h = \left(\frac{E_{sh}}{E_{sv}}\right)\frac{\upsilon_{sv}}{(1-\upsilon_{sh})}\left(S_v - \alpha_v P_p\right) + \left(\alpha_h P_p\right), \quad (3)$$

where $\frac{E_{sh}}{E_{sv}}$ is Young's Modulus (or anisotropic modulus) from triaxial core measured in the horizontal and vertical directions, $\frac{\upsilon_{sv}}{(1-\upsilon_{sh})}$ is the anisotropic bound Poisson's ratio from triaxial core measured in the horizontal and vertical directions, as is α_h and α_v, respectively which define the anisotropic Biot's coefficient. This data in log form represent anisotropic components of the mechanical earth model shown in Figure 4.

The difference in magnitude between the isotropic and anisotropic bound Poisson's ratio (BPR) can then be calculated to represent an Anisotropic Correction Scalar (ACS) magnitude that's applied to the isotropic Closure Stress Scalar (CSS) defined in Equation 2 which now becomes:

$$\mathrm{CSS_{ANI}} = \mathrm{C}\frac{\lambda}{\lambda+2\mu} = \frac{\upsilon_{sv}}{(1-\upsilon_{sh})}, \quad (4)$$

where C is the ACS which equals the isotropic BPR less any anisotropic effects (when C=1). Equation 4 defines the CSS corrected for VTI media, and can now be inserted into Equation 3 and minimum horizontal stress S_h solved for using CSS extracted from the AVO inverted seismic where:

$$\mathrm{S_h} = \left(\frac{\mathrm{E_{sh}}}{\mathrm{E_{sv}}}\right) * \mathrm{C}\frac{\lambda}{\lambda+2\mu}\left(\mathrm{S_v} - \alpha_v \mathrm{P_p}\right) + \left(\alpha_h \mathrm{P_p}\right). \quad (5)$$

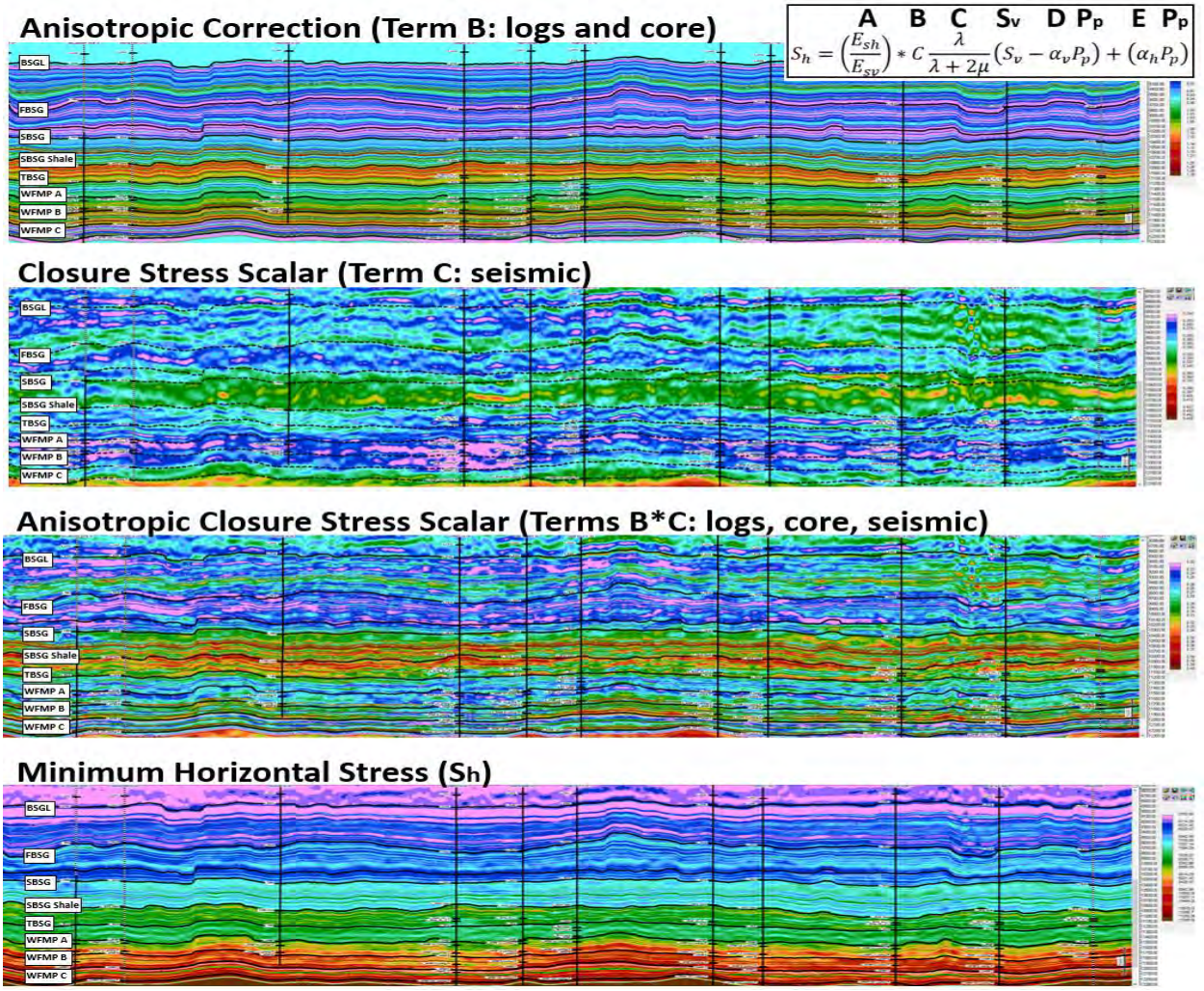

Figure 7 A regional arbitrary cross section from the Delaware Basin study area is shown with vertical wells used to tie the structural framework. Formations are labeled. For all cross sections and maps, hot red / yellow colors define areas of greater in-situ stress (more ductile) and cooler blue / purple colors define relatively less stress (more "brittle"). The top cross section represents anisotropic correction scalars from static triaxial core and dynamic log data. The second panel from top shows Closure Stress Scalar (CSS) from AVO seismic inversion only. The third panel shows the anisotropic corrected seismic (integrating the top two sections) defining the rock quality term. The bottom panel shows the final anisotropic minimum horizontal stress (Sh) solution with pressure gradients. Notice the added geomechanical variability the seismic provides.

Results (qualitative): Delaware Basin

Figure 4 defines the Mechanical Earth Model (or MEM) representing the Delaware Basin study and area, and relates mineralogy and lithofacies to geomechanics and rock physics defined in Figure 2 and 3. The MEM defines overburden stress and pore pressure gradients calibrated to Diagnostic Fracture Injection Tests (DFIT) and dynamic log measurements (Narasimhan, et al., 2016; Cherian, 2018 et al.), and assumes Vertical Transverse (VTI) media representing anisotropic shale (Sayers, 2010). All terms defined in Equation 5 are shown in log form and equally depth sampled at 1 ft. including the CSS volume derived from AVO seismic inversion.

Excluding the seismic defined closure stress scalar, all terms from Equation 5, that define the MEM in Figure 4, were simply interpolated away from the MEM location to areas of interest using the depth converted seismic framework (Shoemaker, et al., 2006) and existing vertical wells as modeling constraints to preserve geologic structure and formation thickness. The end result is seven 3D rock property cubes (Figure 5) representing each of the terms defined in Equation 5 with each cube sampled equally at 1ft., including the seismic defined closure stress scalar term. An identical workflow was completed for the Midland Basin; see Shoemaker et al. (2019) for additional details and results. A final minimum horizontal stress (S_h) cube representing the Delaware Basin study area is shown in Figure 6 which is approximately 30 square miles for perspective. Sub-volumes of the cube, representing multi well

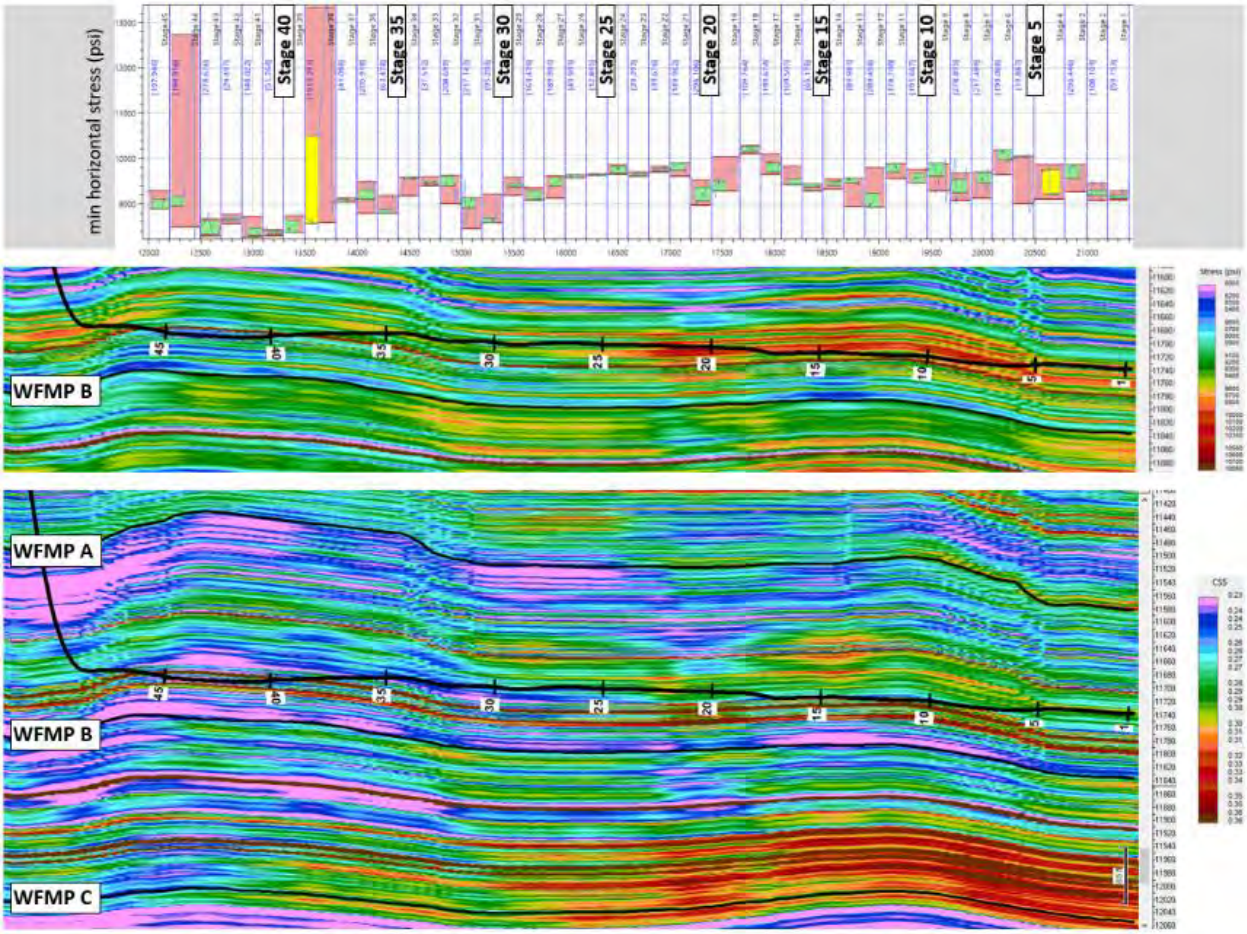

Figure 8. A Delaware Basin arbitrary cross section along a 10,000+ ft. lateral is shown. The wellbore was landed in the lower Wolfcamp A. Minimum horizontal stress form the Sh cube (Figure 6) was extrapolated along the wellbore (middle panel) and input into completion analysis software (top panel) to test cluster and stage spacing sensitivities based on stress differentials defined by lithology / stress contrasts (Figure 9). The bottom panel is the bound Poisson's ratio (or CSS rock quality term) without pore pressure or overburden stress gradients. Vertical resolution is defined at 1 ft. For all cross sections and maps, hot red / yellow colors define areas of greater in-situ stress (more ductile) and cooler blue / purple colors define relatively less stress (more "brittle"). Notice the mechanical variability the seismic provides.

pads for example, can now be carved-out and input directly into fracture geometry simulators in 3D space. Geometries representing stimulated rock volumes can be calculated for optimized treatment design. An example arbitrary regional cross-section miles in length, with the horizon framework, is displayed (Figure 7), and shows the integration-sequence from S_h calculated from core and logs only (top Panel) to the final S_h solution (bottom Panel) which combines the stress variability measured from the seismic inversion.

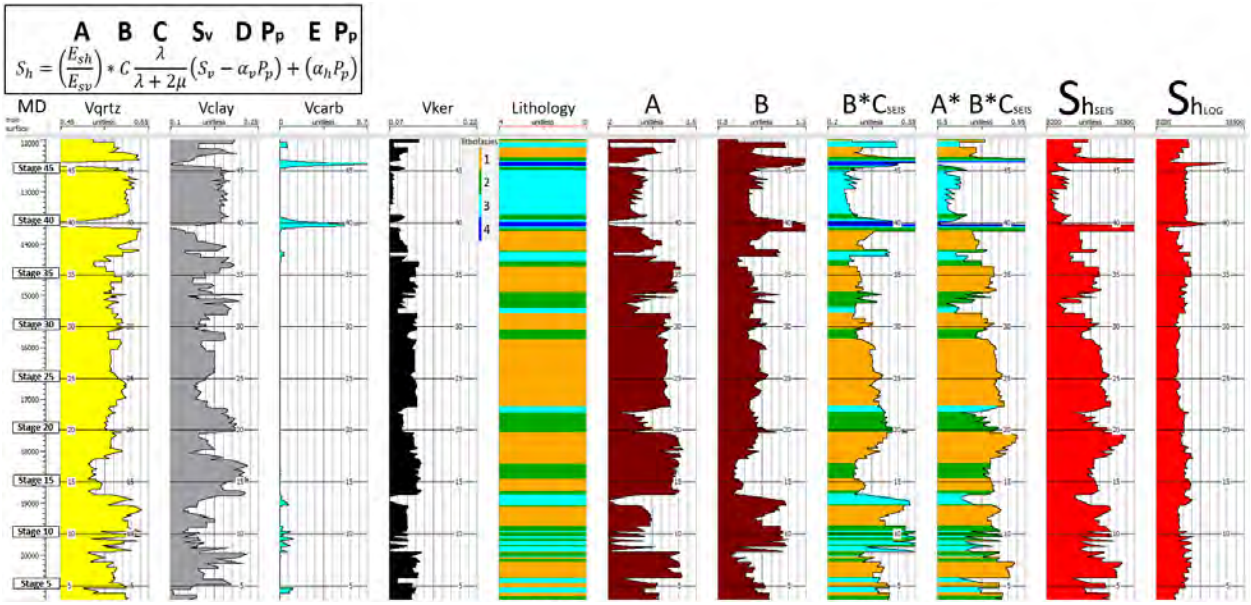

Figure 9. Horizontal logs extracted from rock property cubes along the horizontal wellbore defined in Figure 8. Mineralogy curves correlate with the lithofacies classification defined in Figure 2. Anisotropy curves representing terms A and B (Figure 4) also correlate with lithofacies (Figure 2) and subsequent stress. Anisotropy increases with clay and organics which subsequently defines differential stress for treatment optimization.

Qualitatively, horizontal rock property logs can be extracted lengthwise along lateral wellbores as inputs for sensitivity testing and parametrization of engineered treatment design for non-geometric stage and cluster spacing. For example at the Delaware Basin study area, Figure 8 shows a horizontal wellbore that was previously fraced and treated. In fact, the core and quad combo data used to calculate the MEM in Figure 4 was acquired in the vertical pilot section of the hole. A full suite of horizontal logs extracted from various rock property cubes (Figure 5) along the horizontal wellbore are shown in Figure 9, and include minerology and lithofacies (Figure 2), anisotropic MEM terms (Figure 4), and a final S_h from the stress cube shown in Figure 6. The horizontal logs (displayed vertically in measured depth) show that the primary driver of anisotropy is the increase in ductile mineralogy components, including clay and particularly organics, which correlate with lithofacies-type 1 (track 5). This is especially evident in the vicinity of stages 20, 25, and 30 where relatively higher minimum horizontal stress has been extracted from the stress cube (track 10), typically characteristic of more planar like fractures. Conversely, quartz rich segments of the wellbore with less organics, proportionally replaced with lime (lithofacies-2 and 3), show low stress areas that are relatively more “brittle”, and likely prone to complex type fracturing.

Stage and cluster spacing sensitivity to horizontal mechanical changes along the wellbore can be seen in the top panel of Figure 8. Relative stress differentials are labeled red, representing identical geometric cluster spacing as opposed to green which show selective engineered spacing. Larger stage spacing results at low stress areas along the wellbore that are more prone to complex fracturing, and are characteristic of less organics and thus less anisotropy (lithofacies-3). Similar correlations between minerology and lithofacies, and stress can be confirmed by the rock physics templates shown in Figure 3 for the Wolfcamp formation.

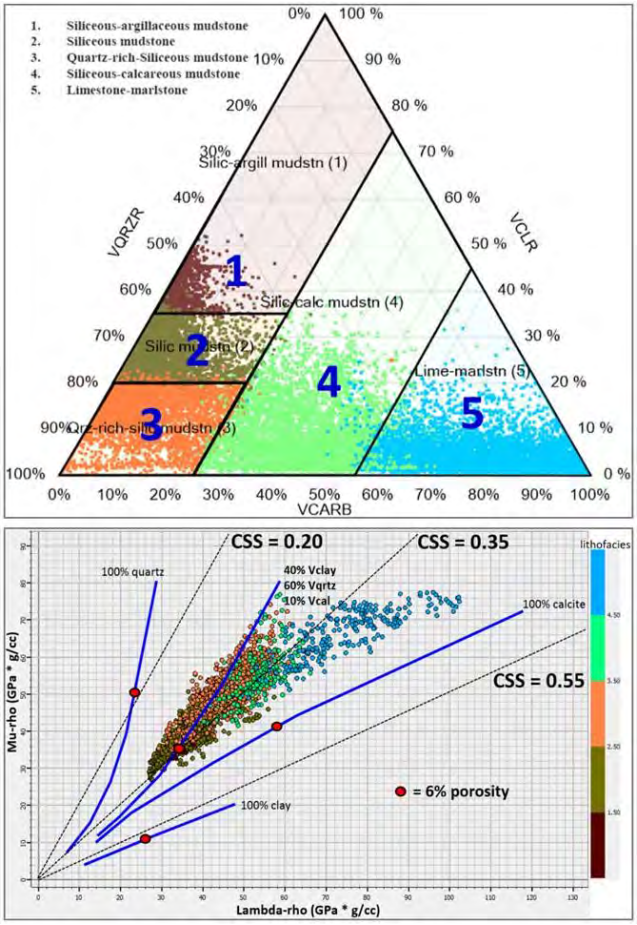

Figure 10. Ternary diagram (top panel) showing lithofacies classification from petrophysics modeling characterizing the Midland Basin study area, and rock physics template integrated with the lithofacies (bottom). See Shoemaker (et al., 2019) for the MEM and log suite used.

Results (quantitative): Midland Basin

For the Midland Basin study area, quantitative in-situ stress maps of the subsurface can now be extracted from a stress cube (Shoemaker, et al., 2019) that represent high risk areas that may be particularly prone to parent-child issues or the well-to-well interference phenomena. Stress maps (Figure 11) outline the area of interest located in the Midland Basin (Figure 1) which has been subdivided into areas representing three horizontal well pads (A, B, and C) that were landed in the upper lower Spraberry (upper map) and the lower Spraberry (bottom map) which are vertically separated by approximately 200 ft. Pads A and B were each developed similarly using a six-well chevron-type pattern (Shoemaker et. al, 2015) with three laterals landed in the upper lower Spraberry (odd numbered wells) and three wells in the lower Spraberry (even numbered wells). Both six-well pads were zipper-fraced with duel frac crews to minimize stress shadowing for enhanced production. Pad C was landed in the lower Spraberry only, and represents a four-well pad drilled significantly earlier than the other pads.

An example regional cross-section in depth (Figure 11) with horizons is displayed from north to south (or from pads A to C) which shows minimum horizontal stress (S_h) calculated from core and logs only (top section), compared to the final S_h solution (bottom section) which integrates the rich geomechanical variability from the CSS seismic. Notice along the cross-sections the two Spraberry landing zones just above the Dean formation which are identified by lateral wells (by pad) for reference. The upper Spraberry landing zone in this part of the basin (wells A5 and B5 from pads A and B) is typically characteristic of higher volume of clay (yellow color), and is thus more ductile representing lithofacies-2 (Figure 10). This increases the induced stress required to fracture the rock by as much as 1,200 psi, greatly influencing fracture geometry and subsequent treatment design for optimal well performance.

Quantitatively, the higher stress effect in the upper zone decreases at northern (blue) areas of the AOI at pad A (Figure 11, top right map) where lower CSS magnitude reflects a greater proportion of carbonate rock vs. clay which is confirmed by vertical wells in the area. Likewise, the lower Spraberry landing also shows relatively more “brittle” rock (bottom map). Consequently, both zones in this part of the basin at pad A represent lithofacies-3 which suggests a less aggressive fracture treatment design with perhaps greater stage and cluster spacing. At pad B however stress maps differ, confirming a much greater in-situ stress for the upper landing zone (top right map, red color) and relatively less stress for the lower landing (bottom right map, purple color). The relatively higher far field stress characteristic of the upper landing may be conducive to increased fracture containment, representing potential areas that may be less prone to “parent-child” depletion issues or areas with less probable well-to-well interference, contrary to (purple) low stress areas that are potentially more prone to asymmetric fracture geometries and well-to-well frac-hits. Acreage can now be high-graded based on said risks, including the potential for production

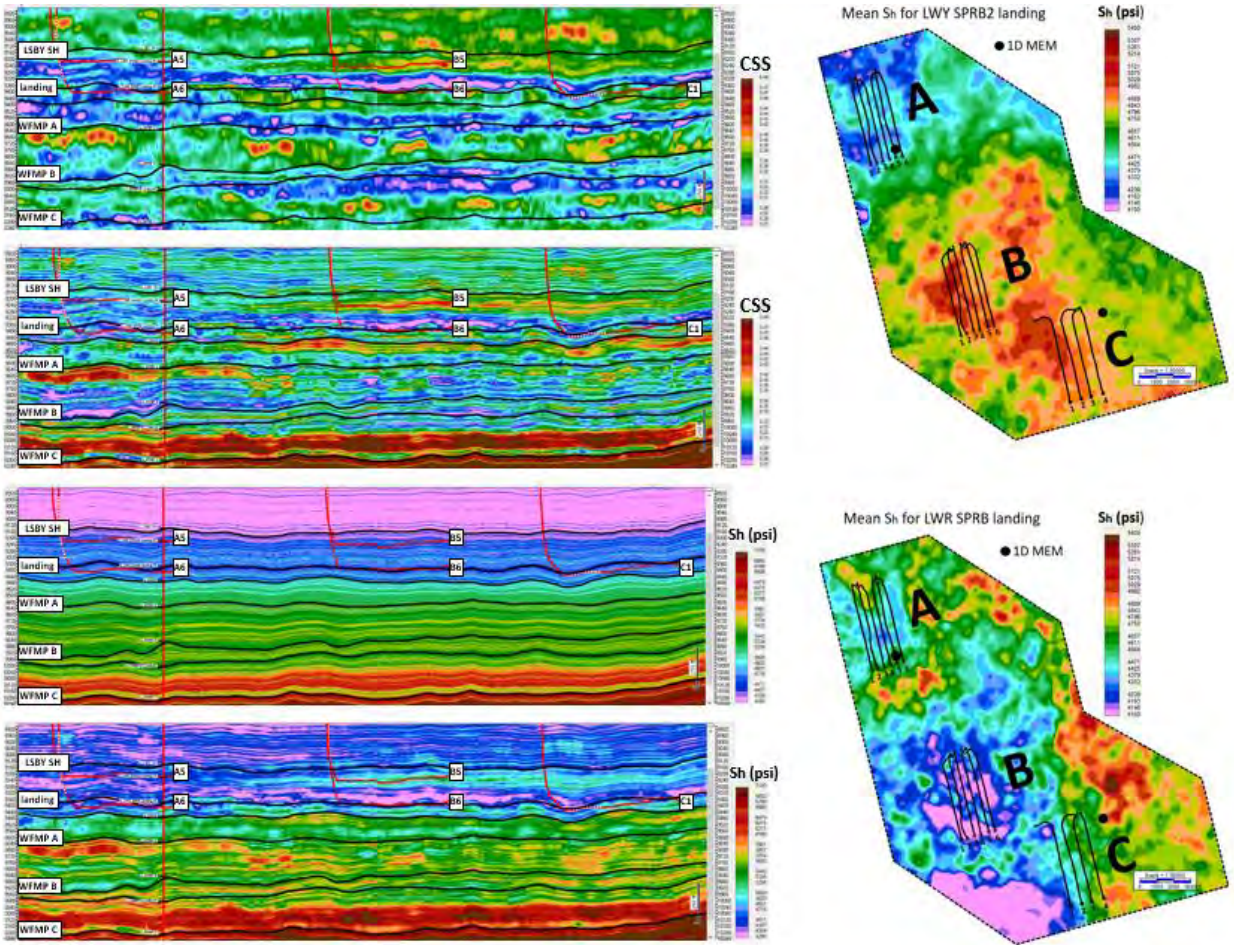

Figure 11 A regional cross section from Permian Basin study area with horizontal wellbores traversing from north to south (from well Pad's A, B, and C). Pads A and B were each developed using a six-well chevron-type pattern with three laterals landed in the upper lower Spraberry (odd numbered wells) and three wells in the lower Spraberry (even numbered wells). Pad C was developed in the lower Spraberry only, and is located near the MEM used for this study area (see Shoemaker et al., 2019). For all cross sections and maps, hot red / yellow colors define areas of greater in-situ stress (more ductile) and cooler blue / purple colors define relatively less stress (more "brittle"). Top Panel shows Closure Stress Scalar (CSS) from AVO seismic inversion only, compared to an identical cross section with anisotropic correction scalars from triaxial core applied (second Panel). The third Panel shows anisotropic minimum horizontal stress (Sh) calculated from core and logs only, compared to the bottom Panel, which shows an identical cross section at log resolution, but integreated with CSS from the AVO seismic. Notice the added geomechanical variability the seismic provides. Also shown are regional (Sh) maps representing the upper Spraberry landing zone (top right) and the lower Spraberry landing zone (lower right).

degradation. Moreover, far field and near wellbore fracture geometry can now be modeled for optimal well spacing and engineered treatment design including stage and cluster spacing based on stress differentials along horizontal wellbores.

The significant vertical stress contrasts, related to the Spraberry landing zones, have also been confirmed by drill cuttings implementing XRD and XRF geochemical analysis for mineralogy compositions along horizontal wells B2 and B3 (at pad B) where cuttings were acquired. Figure 12 summarizes these results and shows that the upper lower Spraberry zone (well B3) does in fact contain by volume up to 30% more clay then the lower Spraberry landing zone. Additional validation from other independent measurements can come from horizontal MWD logs and drilling data with an example shown in Figure 13 from well A6 (pad A) from the lower Spraberry landing zone. While drilling in the Midland Basin, greater ROP values generally correspond to higher clay volumes encountered along the lateral which incidentally is confirmed by greater gamma ray measurements and volume of clay from cuttings where higher in-situ stress states exist from the geomechanics. Development strategies, involving acreage prioritization, can now be optimized regionally, governed by in-situ stress variability.

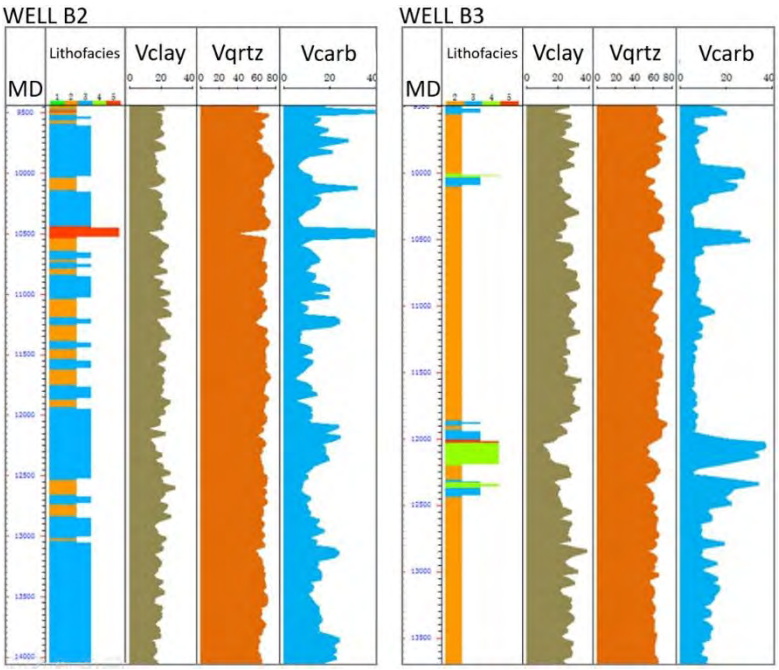

Figure 12 XRD and XRF geochemical analysis of cuttings show minerology compositions by volume for horizontal wells B2 (lower Spraberry landing) and B3 (upper Spraberry landing) located at well pad B (Figure 11) of the Permian Basin study area. Well B2 is characteristic of lithofacies-3 (Figure 10) compared to well B3 which on average shows 30% more clay and represented by lithofacies-2 with subsequent higher stress and ductility requiring a more aggressive fracture treatment.

At present, other seismic methods assume isotropy and do not necessarily account for anisotropy stress in shale formations (Thomsen et al., 2013; Sayers et al., 2015) which can result in significant errors when estimating geomechanical properties resulting in suboptimal treatment design. For example, Figure 14 shows cross sections along well C4 (pad C) landed in the Lower Spraberry of the Midland Basin. Notice that the isotropic CSS, calculated from both seismic and logs (top panels), underestimates anisotropy and hence closure stress values at flooding surfaces (e.g., WFMP A, B, and C) representing organic-clay rich source rocks (lithofacies-1and 2). Increased stress values (from static triaxial core) result after anisotropy scalar corrections are applied to the isotropic values.

Direct application of the method herein is further summarized in Figures 15 and 16 which focus on the six wells representing pad B (Figure 11, see maps), again in the Midland Basin. A minimum horizontal stress (S_h) cross-section in depth (Figure 15) was extrapolated from the S_h volume (see Shoemaker et al., 2019) lengthwise along wellbores B5 and B6 representing the upper lower and lower Spraberry landing zones, respectively. In this case, vertical and lateral in-situ stress

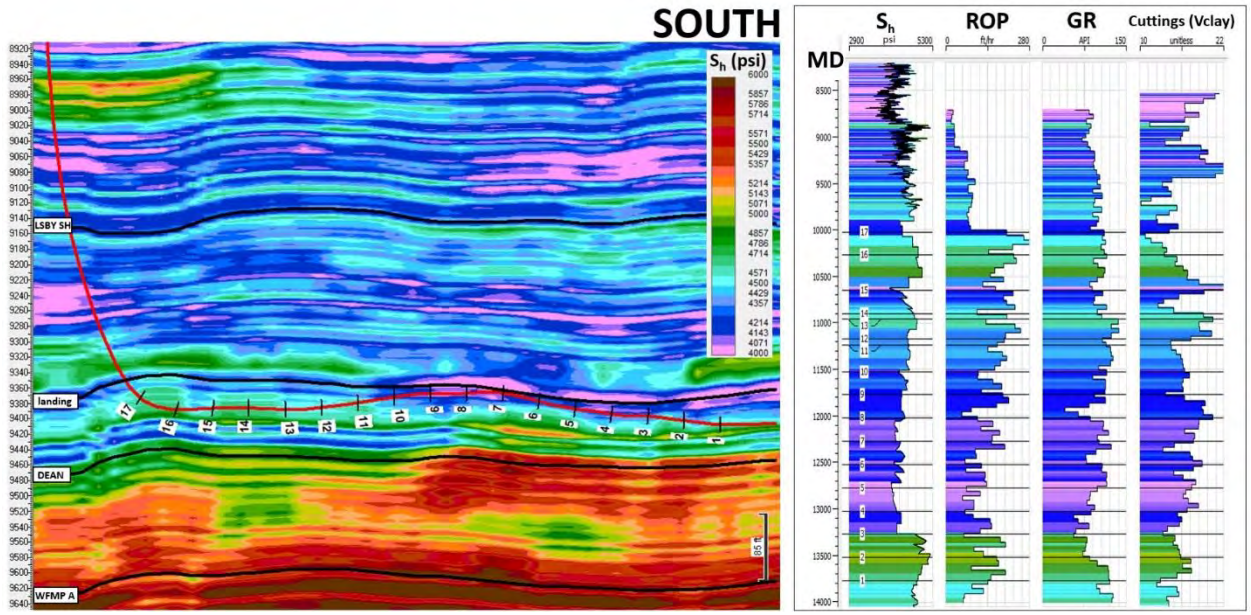

Figure 13 Minimum horizontal stress (Sh) cross section (left panel) lengthwise along horizontal well A6 (Pad A), and independent measurements (right panel) comparing (Sh) extracted horizontally along the wellbore in MD compared to: 1) the rate of penetration (ROP), 2) MWD gamma ray (GR), and 3) volume of clay from XRD and XRF geochemical analysis. Drill bit ROP typically increases within relatively larger volumes of clay horizontally, representing higher stress and Gamma Ray measurements which are shown.

can vary by as much as 2,000 psi vertically from the wellbores and far field which is confirmed by the stress maps representing the landing zones. This is particularly apparent from the cross section at the Dean surface which can act as a frac barrier to downward propagating hydraulic fractures initiated from the lower landing zone. As mentioned above, the significant in-situ stress contrast between the upper and lower landing zones is also apparent in the cross section, which can vary by as much as 1,200 psi. This vertical difference in stress results from the change in elastic properties from the addition of clay and organics. Black curves represent vertical stress logs (Figure 15) extracted from the stress cube.

Lateral contrasting stress states (or horizontal differential stress) can also affect fracture propagation and geometry. Stress maps (Figure 15, right panels) representing the multi well pad landing zones which show

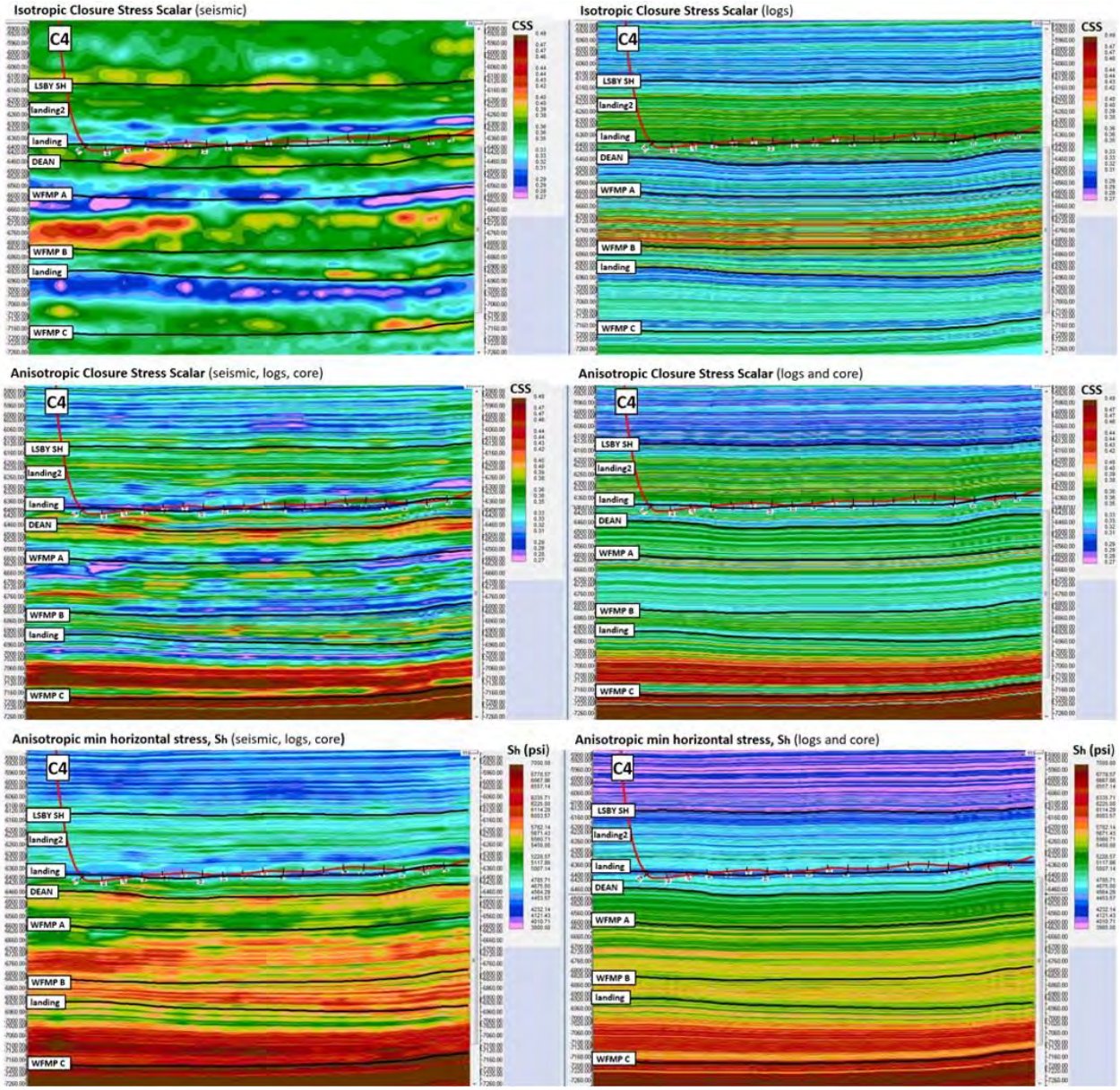

Figure 14. An arbitrary cross section extracted along horizontal well C4 at Pad C (Figure 11). The top-left Panel shows the isotropic Closure Stress Scalar (CSS) from AVO seismic inversion compared to CSS calculated form dynamic logs only (top right Panel). Middle-left Panel shows CSS from AVO seismic corrected for anisotropy effects using scalar terms A and B (Equation 5), compared to the same cross section but with CSS calculated from logs only (middle-right, Panel). The bottom-left Panel compares minimum horizontal stress (Sh) calculated with CSS from AVO seismic inversion compared to (Sh) calculated from CSS using logs only (right Panel). Notice the added geomechanical and stress variability provided by the seismic (left panels). Both Spraberry landing zones are shown as well as the Wolfcamp B landing.

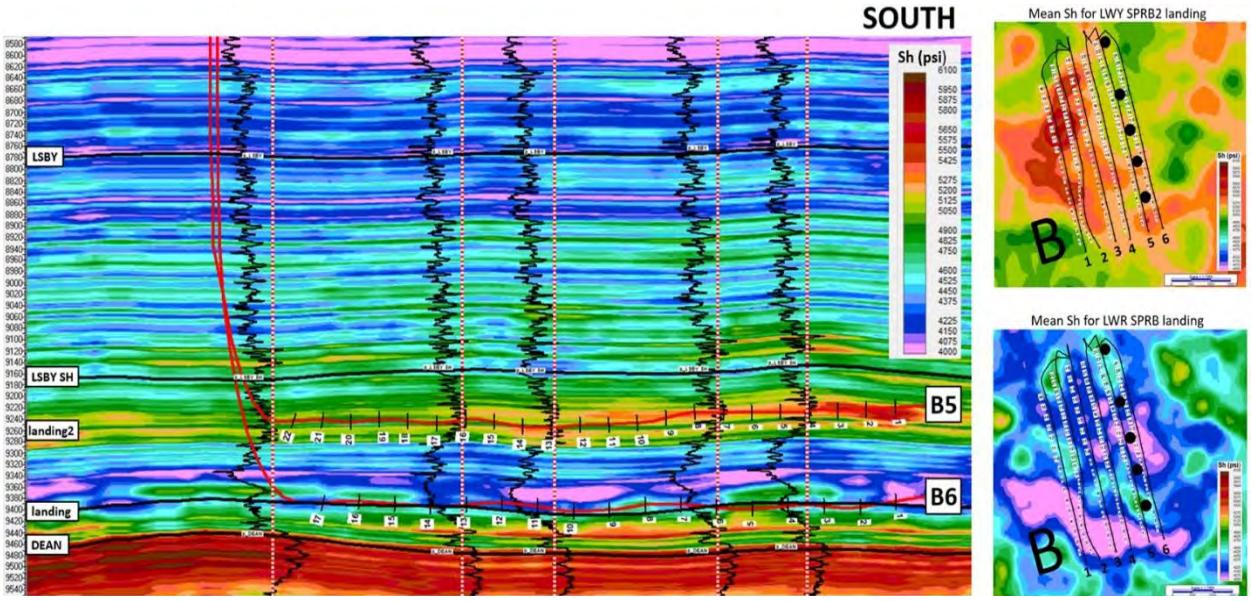

Figure 15. A Cross section representing minimum horizontal stress (Sh) at 1 ft. vertical log resolution along the B5 and B6 horizontal wellbores (Pad B, Figure 11) representing the upper lower Spraberry and lower Spraberry landing zones, respectively. Maps show the Sh variability between the two landing zones, reflecting the significant stress contrast seen in the cross section. Pad B was developed using a six-well chevron-type pattern with three laterals landed in the upper lower Spraberry (odd numbered wells) and three wells in the lower Spraberry (even numbered wells). For all cross sections and maps, hot red / yellow colors define areas of greater in-situ stress (more ductile) and cooler blue / purple colors define relatively less stress (more "brittle").

significant horizontal stress variability potentially affecting the complexity of fracture initiation, length, and height. The maps show the potential for fracture asymmetry, particularly within (purple) areas of low stress toward the toe of the lower Spraberry wells (B2, B4, and B6). For example, less aggressive fracture stimulation at these areas is likely warranted to minimize asymmetry fracture propagation effects, which can cause frac-hits and could be accounted for in designing treatments.

Figure 16 shows fracture geometry models that were run using identical treatment designs to show stress related lithology effects, and were initiated in each of the lower Spraberry landing zones. The lower zone models a fracture geometry with a higher frac height and length relative to the upper lower zone which shows a less efficient frac. As mentioned, the upper zone contains in upwards of 30% more clay (lithofacies-2), thus requiring a more aggressive frac with tighter stage and cluster spacing. This is further substantiated from the hydrocarbon production model (Figure 16, lower right) which was completed using identical treatment designs for both zones, and further demonstrates a more optimal frac with enhanced production from the lower zone due to improved geomechanics that support a less aggressive treatment design relative to the upper landing zone.

Conclusions

Anisotropic minimum horizontal seismic stress volumes presented herein have been corrected for anisotropy using triaxial core, and can be directly input into fracture geometry simulators with the necessary far field and virgin geomechanical variability. Most current methods used to infer subsurface stress are non-unique and more diagnostic, and thus require calibration to existing data, and measure, for example, indirect data representing frac-hits from offsetting wells. Other methods represent workflows that require propagation of geomechanical properties away from vertical well control. However, said methods infer measurements that do not represent rock properties at the area of interest, particularly in 3D space.

The method presented herein successfully integrates multi-domain data sets with 3D seismic expressed in terms of Lamé elastic parameters for added horizontal and vertical elastic variability, and effectively

measures far field stress in 3D space for fracture geometry modeling and fracture treatment optimization away from the wellbore. The stress volume can be interpreted qualitatively for wellbore stability applications and for hydraulic fracture treatment design for engineered optimization and quantitatively for optimal field development strategies including vertical and lateral well spacing, and can be used particularly as a mitigation / prevention tool ahead of the drill bit in areas effected by parent-child and frac hit issues.

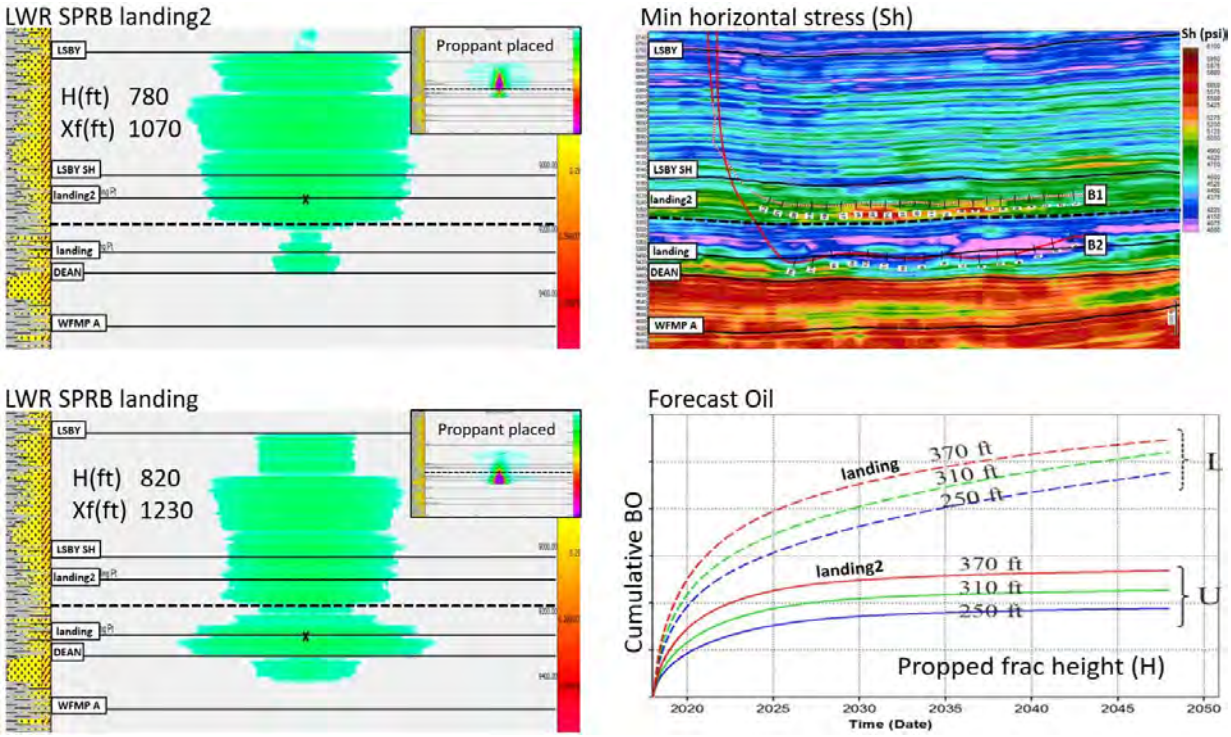

Figure 16. Fracture geometry models run using identical hydraulic fracture treatment designs representing the upper lower Spraberry landing zone (top-left) and the lower Spraberry landing zone (bottom-left), representing wells B1 and B2 (top-right cross section). Vertical depth exaggeration of fracture models and cross section are the same for comparison. The bottom-right panel shows modeled hydrocarbon production of the two landing zones using identical treatment designs. The top profile highlights more production from the lower Spraberry landing zone characteristic of ideal geomechanics (lithofacies-3, Figure 10) and brittleness (less clay and organics, and thus stress) relative to the upper landing zone representing lithofacies-2 which contains more clay for added ductility and stress, and thus requires a more aggressive frac design with tighter stage and cluster spacing to enhance production.

Acknowledgements

The authors would like to thank Callon Petroleum for the permission to publish this work, and to CORDAX for the use of their completion analysis software.

References

Aki, K., and P. G. Richards, 1980, Quantitative seismology:
Theory and methods, 1: W. H. Freeman and Co.

Azad, A., Somanchi, K., Brewer, J. R., & Yang, D. (2017, January 24). Accelerating Completions Concept Select in Unconventional Plays Using Diagnostics and Frac Modeling. Society of Petroleum Engineers. doi:10.2118/184867-MS

Barree, R. D., Gilbert, J. V., & Conway, M. (2009, January 1). Stress and Rock Property Profiling for Unconventional Reservoir Stimulation. Society of Petroleum Engineers. doi:10.2118/118703-MS

Cherian, B. V., McCleary, M., Fluckiger, S., Nieswiadomy, N., Bundy, B., Edwards, S., Shaikh, H. (2015, October 20). Production Performance in the In-Fill Development of Unconventional Resources. Society of Petroleum Engineers. doi:10.2118/175963-MS

Cherian, B., Shoemaker, M., Nwoko, S., Narasimhan, S., Olaoye, O., Iqbal, J., Zakhour, N. (2018, August 28). Understanding Development Drivers in Horizontal Wellbores in the Midland Basin. Society of Petroleum Engineers. doi:10.2118/191782-MS

Cipolla, C. L., Fitzpatrick, T., Williams, M. J., & Ganguly, U. K. (2011, January 1). Seismic-to-Simulation for Unconventional Reservoir Development. Society of Petroleum Engineers. doi:10.2118/146876-MS

Close, D., Parez, M., Goodway, B., and Purdue, P. (2012). "Integrated workflows for shale gas and case study results for the Horn River Basin, British Columbia, Canada." The Leading Edge, 31(5), 556-569.

Cunningham, N., 2018. Why U.S. Shale May Fall Short of Expectations: https://oilprice.com/Energy/Crude-Oil/Why-US-Shale-May-Fall-Short-Of-Expectations.html, accessed November 11 2018.

Dvorkin, J., and Nur, A. (1996). "Elasticity of high-porosity sandstones: Theory for two North Sea data sets." GEOPHYSICS, 61(5), 1363-1370.

Frenzel, H.N. et al., 1988, The Permian Basin region, in Sloss, L.L. ed., Sedimentary cover - North American craton: Geological Society of America, The Geology of North America, v. D-2, p. 261-289.

Galloway, W.E., Ewing, T.E., Garrett, C.M., Tyler, N., and Bebout, D.G., eds., 1983, Atlas of major Texas oil reservoirs - Ellenburger Fractured Dolomite: The University of Texas at Austin, Bureau of Economic Geology, p. 89-93.

Ganpule, S. V., Srinivasan, K., Izykowski, T., Luneau, B. A., & Gomez, E. (2015, February 3). Impact of Geomechanics on Well Completion and Asset Development in the Bakken Formation. Society of Petroleum Engineers. doi:10.2118/173329-MS

Goodway, B. (2010). "The magic of Lamé." The Leading Edge, 29(11), 1432-1432

Goodway, B., Perez, M., Varsek, J., Abaco, C. (2010). "Seismic petrophysics and isotropic-anisotropic AVO methods for unconventional gas exploration." The Leading Edge, 29(12), 1500-1508.

Goodway, B., Chen, T., and Downton, J. (1997) Improved AVO fluid detection and lithology discrimination using Lamé petrophysical parameters; "λρ","μρ",&"λ/μ fluid stack", from P and S inversions. SEG Technical Program Expanded Abstracts 1997: pp. 183-186.

Gray, D. (2002) Elastic inversion for Lamé parameters. SEG Technical Program Expanded Abstracts 2002: pp. 213-216.

Higgins, S. M., Goodwin, S. A., Donald, adam, Bratton, T. R., & Tracy, G. W. (2008, January 1). Anisotropic Stress Models Improve Completion Design in the Baxter Shale. Society of Petroleum Engineers. doi:10.2118/115736-MS

Hobson, J. P., Caldwell, C. D., and Toomey, D. F., 1985a, Early Permian deep-water allochthonous limestone facies and reservoir, west Texas: American Association of Petroleum Geologists Bulletin, v. 69, p. 2130–2147.

Iverson, W. P. (1995, January 1). Closure Stress Calculations in Anisotropic Formations. Society of Petroleum Engineers. doi:10.2118/29598-MS

Jacobs, T., 2019. To solve frac hits, unconventional engineering must revolve around them. Journal of Petroleum Technology, v71, issue 4.

Ma, Y., Holditch, S., 2016, Unconventional Oil and Gas Resources Handbook: Elsevier, e-book.

Mata, D., Dharwadkar, P., Gonzales, V., Sitchler, J., & Cherian, B. (2014, April 17). Understanding the Implications of Multiple Fracture Propagation in Well Productivity and Completion Strategy. Society of Petroleum Engineers. doi:10.2118/169557-MS

Mazzullo, S. J., and Reid, A. M., 1987, Basinal Lower Permian facies, Permian Basin: part II—depositional setting and reservoir facies of Wolfcampian–lower Leonardian basinal carbonates: West Texas Geological Society Bulletin, v. 26, no. 8, p. 5–10.

Miller, C. K., Waters, G. A., & Rylander, E. I. (2011, January 1). Evaluation of Production Log Data from Horizontal Wells Drilled in Organic Shales. Society of Petroleum Engineers. doi:10.2118/144326-MS

Narasimhan, S., Shaikh, H., Gray, J. K., Cherian, B. V., Olaoye, O., Rifai, R., Sharf-Aldin, M. (2016, February 1). Effect of Horizontal Stress Models and Biot Poro-Elasticity on Predicted Fracture Geometry. Society of Petroleum Engineers. doi:10.2118/179162-MS

Perez, M., Goodway, B., Purdue, G., 2012, Stress estimation through seismic analysis: 82nd Annual International Meeting, SEG, Expanded Abstracts, pp. 1949-1954, https://doi.org/10.1190/segam2012-1480.1

Sayers, C. M., Fisher, K., & Walsh, J. J. (2015, December 17). Rock Physics of the Eagle Ford Shale. Society of Exploration Geophysicists.

Sayers, C. M. (2010, January 1). The Effect of Anisotropy On the Young's Moduli And Poisson's Ratios of Shales. Society of Exploration Geophysicists.

Shoemaker, M., Narasimhan, S., Quimby, S., Hawkins, J. (2019, February), Calculating far field anisotropic stress from 3D seismic; The Leading Edge 38, 2 (2019); pp. 96-105, https://doi.org/10.1190/tle38020096.1

Shoemaker, M., Peacock, J., Becher, J., Lacy, J., Zakhour, N. (2018, May), Development Optimization of Horizontal Wellbores Using Lamé Elastic Constants from 3D Seismic within the Permian Basin: Amer. Assoc. of Petr. Geol. (AAPG) Annual Conference, Abstracts, (Salt Lake City, Utah).

Shoemaker, M., Zakhour, N., & Peacock, J. (2015, July 20), Integrating 3D Seismic and Geomechanical Properties with Microseismic Acquisition and Fracturing Parameters to Optimize Completion Practices within the Wolfcamp Shale Play of the Midland Basin. Unconventional Resources Technology Conference (URTeC), Annual Conference, San Antonio, Texas, URTEC-2154184-MS.

Shoemaker, M., Hill, W., Trumbly, P., 2006, Implications of Wavelet Analysis to Reservoir Quality and Reserve Estimation with an Example Case Study from the Deep Trend: 76th Ann. Internat. Mtg., Soc. Expl. Geophys. (SEG), Expanded Abstracts, (New Orleans, Louisiana).

Singleton, S., 2018a, Geophysical data processing, rock property inversion, and geomechanical model building in a Midland Basin development project, Midland/Ector counties, Texas; The Leading Edge 37, 3 (2018); pp. 182-189, https://doi.org/10.1190/tle37030182.1.

Singleton, S. 2018b, Integration of Geophysics and Engineering for Geomechanical Earth Modeling in a Midland Basin Development Project, Midland/Ector Counties, Texas. Unconventional Resources Technology Conference, Houston, Texas, 23-25 July 2018: pp. 1723-1728.

Thiercelin, M. J., & Plumb, R. A. (1994, December 1). A Core-Based Prediction of Lithologic Stress Contrasts in East Texas Formations. Society of Petroleum Engineers. doi:10.2118/21847-PA

Thomsen, L. (2013, January 1). On the use of Isotropic Parameters λ E, v, K to Understand Anisotropic Shale Behavior. Society of Exploration Geophysicists.

U.S. Energy Information Administration, 2018. Permian Region is Expected to Drive U.S. Crude Oil Production Growth through 2019: https://www.eia.gov/todayinenergy/detail.php?id=36936, accessed November, 2018.

U.S. Energy Information Administration, 2019, Petroleum & Other Liquids; Monthly Drilling Productivity Report, released April 15, 2019.

Vernik, L., and J. Milovac, 2011, Rock physics of organic shales; The Leading Edge, Vol. 30 #3, pp. 318-322. https://doi.org/10.1190/1.3567263

Vernik, L., 2016, Seismic Petrophysics in Quantitative Interpretation: SEG, e-book.

Warpinski, N. R., & Teufel, L. W. (1987, February 1). Influence of Geologic Discontinuities on Hydraulic Fracture Propagation (includes associated papers 17011 and 17074) Society of Petroleum Engineers. doi:10.2118/13224-PA

Wilson, J. L., 1975, Carbonate facies in geologic history: New York, Springer-Verlag, 471 p

Zoeppritz, K., (1919), Erdbebenwellen VII, VII B, ÜberReflexion und Durchgang seismischer Wellen durch Unstetigkeitsflächen [On the reflection and transmission of seismic waves at surfaces of discontinuity]: Nachrichten von der Königlichen Gesellschaft Wissenschaften zu Göttingen, Mathematischphysikalische Klasse, 66–84.